

Gray Platelet Syndrome: Pro-inflammatory megakaryocytes and α -granule loss cause myelofibrosis and confer resistance to cancer metastasis in mice

Running head: NBEAL2 and gray platelets beyond hemostasis

Jose A. Guerrero^{1,2}, Cavan Bennett^{1,2}, Louise van der Weyden³, Harriet McKinney^{1,2}, Melody Chin^{1,2}, Paquita Nurden⁴, Zoe McIntyre³, Emma L. Cambridge³, Jeanne Estabel³, Hannah Wardle-Jones³, Anneliese O. Speak³, Wendy N. Erber⁵, Augusto Rendon^{1,2}, Willem H. Ouwehand¹⁻³, Cedric Ghevaert^{1,2}

¹Department of Haematology, University of Cambridge, Cambridge Biomedical Campus, Cambridge, United Kingdom.

²NHS Blood and Transplant, Cambridge Biomedical Campus, Cambridge, United Kingdom.

³Wellcome Trust Sanger Institute, Wellcome Trust Genome Campus, Hinxton, Cambridge, United Kingdom.

⁴Institut Hospitalo-Universitaire LIRYC, Hopital Xavier Arnoz, Pessac, France.

⁵Pathology and Laboratory Medicine, University of Western Australia, Crawley, Western Australia, Australia.

Correspondence to:

Jose A Guerrero (jg652@medschl.cam.ac.uk) and Cedric Ghevaert (cg348@cam.ac.uk)

University of Cambridge / NHS Blood and Transplant. Cambridge Blood Centre.

Long Road, CB2 0PT, Cambridge, UK.

Tel: +44 1223 588095 // +44 1223 588082 // Fax: +44 1223 588155

Text Word Count: 4189// Abstract Word Count: 133 // Number of Figures: 7 // Number of References: 48

Scientific category: Platelets and Thrombopoiesis

Key Points:

1. Pro-inflammatory megakaryocytes from mice with Gray Platelet Syndrome drive the extension of myelofibrosis, splenomegaly and emperipolesis.
2. The lack of pre-formed alpha-granules in *Nbeal2*^{-/-} platelets leads to protection against cancer metastasis.

Abstract

NBEAL2 encodes a multidomain scaffolding protein with a putative role in granule ontogeny in human platelets. Mutations in *NBEAL2* underlie Gray Platelet Syndrome (GPS), a rare inherited bleeding disorder characterized by a lack of α -granules within blood platelets and progressive bone marrow fibrosis. We present here a novel *Nbeal2*^{-/-} murine model of GPS and demonstrate that the lack of α -granules is due to their loss from platelets/mature megakaryocytes, and not by initial impaired formation. We show that the lack of *Nbeal2* confers a pro-inflammatory phenotype to the bone marrow megakaryocytes, which in combination with the loss of proteins from α -granules drives the development of bone marrow fibrosis. In addition, we demonstrate that α -granule deficiency impairs platelet function beyond their purely hemostatic role and that *Nbeal2* deficiency has a protective effect against cancer metastasis.

Introduction

Platelets are anucleate cells that circulate in the blood and their primary role is in hemostasis. They are also essential in processes such as inflammation¹, angiogenesis², and wound healing³ and contribute to the pathogenesis of myocardial infarction, stroke⁴, rheumatoid arthritis⁵, and malignant metastasis^{6,7}. This myriad of actions is explained in part by the unique cargo of their alpha (α) and dense (δ) granules. A vast array of more than 300 proteins is stored in the α -granules⁸ including hemostatic and adhesive molecules, such as von Willebrand Factor (VWF), fibrinogen and other coagulation factors, inflammatory peptides like IL1B, TGF β , RANTES and pro- and anti-angiogenic factors such as VEGF, PDGF, PF4 and THBS1⁹.

Platelets contain 30-50 α -granules which account for approximately 10% of their volume⁹. Alpha-granules are formed early during megakaryopoiesis by the fusion of small vesicles from the trans-Golgi network and endocytic vesicles into multivesicular bodies (MVBs)¹⁰ then transported through the cytoplasmic extensions of the proplatelet shafts of the mature megakaryocytes (MKs), the bone-marrow residing platelet precursors, where they become trapped in the terminal buds, i.e. the nascent platelets^{11,12}.

Gray platelet syndrome (GPS), is a rare autosomal recessive bleeding disorder first reported in 1970¹³ caused by mutations in *NBEAL2*¹⁴⁻¹⁶. Platelets from GPS patients are large and have a gray appearance caused by an almost complete absence of α -granules. However some platelets contain MVBs and occasionally platelets with sparse α -granules are seen¹⁷. Other organelles such as mitochondria, δ -granules and lysosomes are unaffected¹⁸. Interestingly nearly all GPS cases develop fibrosis of the bone marrow in the fourth to fifth decade of life¹⁸ possibly as a consequence of the steady release of cytokines, chemokines and growth factors normally packaged in the α -granules.

NBEAL2 belongs to a family of genes encoding the BEACH-domain containing proteins¹⁴. Most of these genes encode large multidomain scaffolding proteins with at least 2,500 amino acids. Besides *NBEAL2* and *GPS*, mutations in other members of this family are also causative of Mendelian disorders of granule ontogeny and the control of cell volume, with mutations in *LYST* causing abnormal lysosomal granules and large neutrophils in Chediak-Higashi Syndrome¹⁹, and a mutation in *NBEA* causing a defect of platelet δ -granules in a case with extreme autism²⁰.

To study the role of *Nbeal2* in α -granule formation and *GPS*-related pathologies, such as myelofibrosis, we generated *Nbeal2* null (*Nbeal2*^{-/-}) mice. We demonstrate that this murine model recapitulates the typical platelet phenotype observed in *GPS* patients including splenomegaly and myelofibrosis. Analysis of the MKs unexpectedly showed that α -granules are generated but not retained within MKs. We also show a strong pro-inflammatory transcriptome signature in MKs from *Nbeal2*^{-/-} mice and interestingly platelets formed by these MKs lack the ability to support metastasis of melanoma cancer cells to the lung. In conclusion, we demonstrate for the first time that deficiency in *Nbeal2* and a lack of α -granules in *GPS* platelets has consequences beyond their primary role in haemostasis.

Materials and Methods

Generation of *Nbeal2*^{-/-} mice

Gene targeting for *Nbeal2* was performed as part of an international consortium (www.knockoutmouse.org) as previously reported²¹⁻²³, and described in Supplemental Methods, and illustrated in Suppl Fig 1A-B.

Adult animals ranging 4-12 months were used including age-matched controls of the same genetic background. Mice were kept in specific pathogen-free conditions, and all procedures were performed according to the United Kingdom Home Office regulations. A minimum of 5 different mice per experiment was used unless otherwise stated.

Platelets and MKs isolation and analysis

Blood was withdrawn from the IVC in either EDTA (5mM final) or ACD (111 mM glucose, 71 mM citric acid, 116 mM sodium citrate) as anticoagulants depending on the experiment. Full blood counts were obtained using a Scil Vetabc instrument (Montpellier, France) and blood smears were stained with a May-Grünwald Giemsa (Romanovsky) stain.

Platelet preparation, culture of bone marrow derived MKs, proplatelet assays, flow cytometry analysis and generation of cell lysates for western blot have been described before and are detailed elsewhere²⁴ and in Supplemental Methods.

Transmission electron microscopy of platelets, bone marrow megakaryocytes and *in vitro*-cultured megakaryocytes

Fixed solutions of platelets, bone marrow-derived and cultured MKs were rinsed in 0.1M HEPES buffer 5 times and processed as described in Supplemental Methods.

Immunostaining of platelets and megakaryocytes

Fixed platelets were incubated onto coverslips at 37 °C for 90 min. Purified cultured MKs were adhered onto fibrinogen-coated slides and then fixed. A detailed description of immunostaining is provided elsewhere²⁵ and in Supplemental Methods.

Analysis of tissue sections

Humerus, femur, tibia, fibula and spleen were taken and placed in a formalin fixative. After decalcification they were processed as stated in Supplemental Methods.

Expression arrays and Q-PCR in cultured MKs

RNA was isolated from cultured MKs using the RNeasy kit (Qiagen, Manchester, UK) and cDNA made using Superscript III or SS VILO (first Strand kit; Invitrogen). Q-PCR assays were performed on a Mx3005P qPCR System (Agilent Technologies, UK) using primers described in Suppl File 1. Expression levels were assayed using Illumina Mus 6v2 expression chip. Data processing and analysis were performed as described elsewhere²⁴. Gene set enrichment analysis was carried out using GSEA²⁶. Version 4 gene sets of GO molecular function were used with a weighted scoring scheme of the t scores.

Experimental metastasis assay

Murine metastatic melanoma B16-F10 cells were cultured in DMEM supplemented with 10% (v/v) fetal bovine serum, 2 mM glutamine and 100U/mL penicillin/streptomycin. Cells in log-phase growth were harvested, resuspended in PBS and 5×10^5 cells (in 0.1 mL) were injected into the tail vein of 6-8 week old sex-matched syngeneic control (n=9) and *Nbeal2*^{-/-} (n=5) mice. Additional groups included *Nbeal2*^{-/-} animals (n=4) transfused with 240×10^6 platelets

previously isolated from control mice, or PBS (n=3) and control mice injected with PBS (n=5) four hours prior to the melanoma cells injection. Mice were sacrificed 10 days later. Lungs were removed, rinsed in PBS and the number of metastatic foci counted under a dissecting microscope.

Statistics

Results are shown as Mean \pm SEM. Statistical analysis was performed using the unpaired Student's t test. P-values under 0.05 were considered statistically significant.

Results

The *Nbeal2*^{-/-} mouse has a Gray Platelet Syndrome phenotype

The absence of *Nbeal2* at transcript and protein level was confirmed in *Nbeal2*^{tm1a Wtsi/tm1a Wtsi} (hereafter referred to as *Nbeal2*^{-/-}) bone marrow-derived MKs and blood platelets (Fig 1A and 1B). The platelet count was reduced by almost 50% ($1,377 \pm 84 \times 10^3$ vs $811 \pm 49 \times 10^3$ platelets/ μ L for control and *Nbeal2*^{-/-} animals, respectively; P-value= 3.1×10^{-7}) (Fig 1C) and the mean platelet volume was increased (5.2 ± 0.1 vs 6.1 ± 0.1 fL; P-value= 8.1×10^{-8}) (Fig 1D), also shown by flow cytometric analysis (Fig 1E), and the “greyish” appearance confirmed (Fig 1F). Crucially, splenomegaly and bone marrow myelofibrosis, clinical features typical of GPS cases, were observed in *Nbeal2*^{-/-} animals older than 9 months (Fig 1G and 1H, respectively).

Nbeal2^{-/-} platelets lack α -granules

Platelet ultrastructure was studied by transmission electron microscopy (TEM). Control platelets had the typical discoid shape and contained numerous α -granules (Fig 2A-B). As expected platelets from *Nbeal2*^{-/-} animals were larger, rounder in shape with some platelets showing abnormal membrane formations with linear or tubular sheets inclusions (Fig 2C-D and Suppl Fig 2). As in human GPS platelets, there was a reduction in α -granule contents. The typical vacuole-like organelles were present, with some containing electro-dense material (Fig 2C-D). The TEM results were confirmed by immunofluorescence staining for α -granule proteins (such as VWF) by confocal microscopy. VWF was shown to have the typical granular distribution in control platelets (Fig 2E) whereas *Nbeal2*^{-/-} platelets either completely lacked VWF (Fig 2F) or displayed a diffuse rather than granular distribution.

Total platelet protein content was analysed by Western Blotting using platelet lysates. Whilst CD63 (LAMP-3), a marker of δ -granules and lysosomes, was present at similar levels in control and *Nbeal2*^{-/-} platelets, there was a significant reduction in α -granule proteins such as VWF, THBS1 and PF4 in the latter (Fig 2G).

We went on to characterize platelet function. First, we carried out flow cytometry analysis to assess the expression of the main platelet receptors on the surface of resting platelets, which showed no differences between groups of control and *Nbeal2*^{-/-} mice for integrin α IIB β 3 (CD41/61), integrin α 2 (CD49b), glycoprotein (GP) V (CD42d) and GPVI (Suppl Fig 3). Engaging platelets with cross-linked collagen-related peptide (CRP) and thrombin showed equivalent levels of activation between groups of animals as determined by the level of fibrinogen binding to α IIB β 3 (Fig 2H top panel), consistent with preservation of the major platelet activation pathways. In contrast, exposure of the α -granule membrane protein P-selectin on the outer surface of platelets after their activation with CRP and thrombin was significantly reduced in *Nbeal2*^{-/-} mice (Fig 2H middle and bottom panels), consistent with the reduction in α -granules.

***Nbeal2*^{-/-} MKs have a maturation defect but proplatelet formation is maintained**

Bone marrow sections from *Nbeal2*^{-/-} and control mice (n=5) were stained with haematoxylin and eosin (H&E) and an immunoperoxidase method for the platelet glycoprotein α IIB β 3 complex (CD41). The number and morphology of the MKs in the bone marrow sections were assessed by a haemato-pathologist who was blinded to the *Nbeal2* status of the mice (Fig 3A). The total number of MKs was comparable in *Nbeal2*^{-/-} and control mice (Fig 3B, top panel). However, *Nbeal2*^{-/-} mice had significantly fewer large MK with multilobated nuclei (Fig 3B, middle panel; P-value=0.038) and an increase in small MKs with reduced nuclear

lobation compared with control mice (Fig 3B, bottom panel; P-value=0.00023). Further, the MKs in *Nbeal2*^{-/-} mice had prominent emperipolesis of neutrophils (Fig 3A); this was not seen in MKs of the control samples. These distinctive MK morphological features enabled all *Nbeal2*^{-/-} and control mice to be identified with 100% accuracy. To further study the potential effects of emperipolesis on MKs, including cell death, immunolabelling of Bcl-XL and cleaved caspase 3 was carried out in bone marrow sections. No difference was observed for either staining between control and *Nbeal2*^{-/-} MKs (Suppl Fig 4).

We then analysed *in vitro* MK differentiation and maturation from bone marrow cultures using two sub-maximal concentrations of thrombopoietin (TPO; 1 and 5 ng/mL) at two time points (3 and 5 days). The number of megakaryocytic CD41⁺ cells was similar in control and *Nbeal2*^{-/-} samples at day 1. However, the difference in the percentage of CD41⁺ cells between control and *Nbeal2*^{-/-} samples gradually increased up to 2.5-fold at day 5 with 5 ng/mL TPO (Fig 3C). In contrast, the proportion of high ploidy MKs (cells with 8N and above) within the CD41⁺ population did not differ between the cultures (Fig 3D).

Proplatelet formation was analysed by adhering bone marrow-derived cultured MKs onto fibrinogen after selection of the most mature MKs ($\geq 8N$) over a BSA gradient. The rate of proplatelet formation was similar in control and *Nbeal2*^{-/-} cells (Fig 3E).

Lack of *Nbeal2* does not affect α -granule formation, packaging or transport to the budding proplatelets

TEM assessment of bone marrow culture-derived MKs showed no major differences between *Nbeal2*^{-/-} cells and controls (Fig 4A-B). In particular there were equal numbers of MVBs, the precursors of α -granules, in both sample sets (Fig 4C-D). As only a few truly mature α -granules were seen in the cultured MKs, we went on to study MKs directly flushed from the

bone marrow. Control MKs showed a well-defined demarcation membrane system (DMS) with the presence of “platelet territories” and mature α -granules (Fig 4E, G, I). *Nbeal2*^{-/-} MKs appeared to have a more rudimentary DMS and a minor degree of vacuolisation but did not show any significant abnormalities such as membrane inclusions (Fig 4F, H, J, K, L). Strikingly, mature α -granules were present in *Nbeal2*^{-/-} MKs and were of similar size and morphology to those in control MKs, although their density and opacity was slightly decreased (Fig 4G-J). The striking emperipolesis documented by light microscopy on bone marrow sections was also observed in *Nbeal2*^{-/-} MKs by TEM (Suppl Fig 5). The presence of α -granules in both control and *Nbeal2*^{-/-} MKs was confirmed by immunohistochemistry. Staining from VWF showed a similar granular distribution in both sets of samples (Suppl Fig 6). In keeping with these observations, western blot analysis of *Nbeal2*^{-/-} and control cultured MK lysates confirmed similar cellular content not only for CD63, but also for α -granule proteins such as VWF, THBS1 and PF4 (Fig 4M).

The apparent discrepancy of these results between the *Nbeal2*^{-/-} platelets and MKs led us to assess whether the lack of *Nbeal2* affects transport and accumulation of granules in the proplatelet buds. To this end we carried out proplatelet assays using mature culture-derived MKs as described above and visualised the proplatelet buds by scanning electron microscopy (SEM), TEM and confocal microscopy (Fig 5A-K). This confirmed the presence of α -granules at different levels of maturation, including MVBs within the cytoplasm of the proplatelet territories in both control and *Nbeal2*^{-/-} samples (Fig 5A-C). Immunolabelling for VWF showed the typical granular distribution previously documented but in particular comparable accumulation of α -granules in the proplatelet buds in both sets of samples (Fig 5D-E). The α -granule content is the result of both intracellular protein synthesis and endocytosis of extracellular proteins, such as fibrinogen. To assess whether the lack of

Nbeal2 potentially affects the latter cellular process, MKs were incubated with FITC-labelled fibrinogen for 24 hours during culture prior to performing the proplatelet assay. FITC-fibrinogen showed a similar granular distribution to that seen for VWF, not only in the core of the cells but also in the proplatelet buds (Fig 5F-G). Co-immunolabelling with other α -granule proteins of endogenous origin, namely P-selectin (Fig 5H-I) and VWF (Fig 5J-K) confirmed that both endogenous and endocytosed proteins accumulate in granules within the terminal buds of both control and *Nbeal2*^{-/-} proplatelets, although segregating in distinct population of granules, a phenomenon which has been previously described²⁷. Additional deconvolved images of the raw confocal stacks were also generated and are available for viewing (Suppl Fig 7 and 8). The number of proplatelets and VWF⁺ proplatelet buds per cell were quantified and revealed no statistically significant differences (Fig 5L-M).

***Nbeal2*^{-/-} MKs have a proinflammatory profile**

Both GPS mice and patients develop premature myelofibrosis of the bone marrow with ageing and it may be that this is caused by the pro-inflammatory nature of GPS MKs and platelets. To provide insights into the role of *Nbeal2* in MKs, we analysed the RNA from culture-derived MKs on gene expression arrays. Analysis showed that 157 genes were differentially expressed with a False Discovery Rate < 0.1. The 25 most differentially expressed transcripts (over-expressed and under-expressed in *Nbeal2*^{-/-}) are listed in Suppl File 2. Absence of *Nbeal2* was confirmed at the transcript level. Term enrichment analysis based on Gene Ontology (GO) molecular function identified 20 gene sets significantly enriched in *Nbeal2*^{-/-} relative to control MKs (FDR < 0.25) (Suppl File 3). The most significant GO term enrichment concerned genes encoding chemokines (Fig 6A). A set of chemokine transcripts (namely *Ccl3*, *Ccl4*, *Cxcl16*, *Cxcl11*, *Cxcl2* and *Cxcl10*) was selected for confirmation testing of the observed transcript level differences by qPCR and all

replicated (Fig 6B). *Ccl3* and *Ccl4* encode Macrophage Inflammatory Protein (MIP) 1 α and 1 β , respectively, well-known pro-inflammatory chemokines increased in primary myelofibrosis^{28,29}, whilst Cxcl1 is a neutrophil chemoattractant³⁰. To determine whether the increased transcript levels were mirrored at the protein level, levels of MIP1 α , MIP1 β and Cxcl1 were determined by ELISA in MK culture supernatant and plasma. MIP-1 α and MIP-1 β levels were higher in the culture supernatant of *Nbeal2*^{-/-} MKs (Fig 6C), and MIP-1 β was significantly increased (P-value=0.0019) in plasma of *Nbeal2*^{-/-} animals at 1 year of age when compared to age-matched controls (Fig 6D).

Alpha-granule deficiency confers protection against cancer metastasis

Platelet function extends beyond hemostasis and we therefore went on to analyze the potential relevance of platelet α -granules in tumorigenesis, and, in particular, metastatic spread. For this we used an *in vivo* model of experimental lung metastasis. Ten days after intravenous injection of murine melanoma B16-F10 cells, lung metastases were quantified. Strikingly, we found a marked reduction, by almost 80%, in the number of pulmonary metastases in *Nbeal2*^{-/-} mice (231 \pm 21 vs 56 \pm 21, P-value= 0.001) (Fig 7). To confirm the key role of platelets and particularly the role of α -granules in metastasis, platelets isolated from control mice were transfused into *Nbeal2*^{-/-} animals prior to injecting the melanoma cells. The platelet count incremented by 119 \pm 20 \times 10⁹/L (P-value<0.05) compared to mice injected with PBS alone and was maintained over the first 48 hours post-transfusion. One of the mice transfused with PBS had to be culled at day 6 and showed no lung metastases. At day10, PBS-control mice had 115 \pm 18 pulmonary metastases, while platelet-transfused and PBS-injected *Nbeal2*^{-/-} animals had 95 \pm 7 and 8 \pm 3, respectively (P-value = 0.004).

Discussion

For over 40 years cellular and biological studies of GPS have been carried out using human samples from clinical cases and therefore most of the reported data relates to the platelet phenotype, due to challenges in isolating abundant MKs from human blood samples. In 2011, three groups reported *NBEAL2* as the gene underlying GPS, and consequently, two reports have been recently published describing an *Nbeal2*^{-/-} mouse model that recapitulates the platelet phenotype observed in human GPS cases^{31,32}. Although our study uses a novel *Nbeal2*^{-/-} mouse with a different genetic strategy, the platelet hallmarks of GPS are recapitulated. In addition we present data that provides a role for *Nbeal2* in platelets beyond their classical hemostatic role. We demonstrate that the lack of α -granules in platelets is the result of an impaired retention rather than a lack of granule generation. In addition, we show that *Nbeal2* deficiency in MKs leads to distinctive pathological findings such as myelofibrosis and a pro-inflammatory phenotype.

In agreement with previous studies^{31,32}, the hemostatic platelet function of *Nbeal2*^{-/-} mice was shown to be similarly impaired. In one study, this was shown to correlate with a decrease in the thrombo-inflammatory process of hypoxic brain damage and impaired wound healing suggesting an effect of platelet α -granule deficiency beyond primary hemostasis. In contrast with the previous mouse models, we observed the development of bone marrow fibrosis and splenomegaly (a feature of human GPS) in older animals. It is well documented that, in the context of myeloproliferative neoplasms (MPNs), pro-inflammatory cytokines play a central role in clinical symptoms and, probably, pathogenicity of the disease²⁹. In the context of JAK2V617F positive myelofibrosis, one of the main benefits of treating patients with JAK2 inhibitors has been the control of inflammation and the raised cytokine levels leading to a resolution of systemic symptoms³³. Transcriptome analysis of cultured MKs

followed by qPCR validation clearly showed that *Nbeal2*^{-/-} MKs overexpress transcripts for several chemokines confirming a link between *Nbeal2* deficiency and inflammation in the context of GPS. Significantly, we found that plasma levels of at least one of those chemokines (MIP-1 β) were raised suggesting a potential systemic effect beyond the bone marrow. Emperipolesis of neutrophils was a prominent feature of the *Nbeal2*^{-/-} marrow, which may be explained through the paracrine effect of chemoattractants such as Cxcl1 released by *Nbeal2*^{-/-} MKs. There is evidence in MPNs that emperipolesis can be driven by an increased level of P-selectin exposure on the surface of MKs which we did not observe in *Nbeal2*^{-/-} MKs and that emperipolesis may induce MK death leading to the release of granule content and subsequent fibrosis³⁴. However, immunolabelling of cleaved Caspase-9 and Bcl-XL in bone marrow showed no differences between mice suggesting that this may not be the case in the context of GPS. Although we cannot rule out that immune cells within the bone marrow participate in the inflammatory phenotype, overproduction of chemokines by MKs in liquid cultures depleted of inflammatory cells suggest that the MKs are one of the primary drivers of inflammation in GPS.

Myelofibrosis in GPS patients may be the result of spontaneous release of α -granule proteins from the MKs¹⁸. One of our most striking observations was the contrast between the circulating platelets, which were almost entirely devoid of α -granules, and the MKs where granule content was preserved. Analysis of the MKs by electron microscopy and immunofluorescence showed normal production/maturation of MVBs and mature α -granules, preserved packaging of both endogenous and endocytosed granule proteins and normal transport of the α -granules to the proplatelet tips. This indicates that the lack of *Nbeal2* does not hamper granule synthesis but suggests lack of retention of α -granules within the cell. It is unclear whether this loss occurs in platelets after their release into the circulation and/or at the level of the MKs within the bone marrow. If the latter, the loss can be compensated by *de*

novo synthesis explaining the similar granule content in control and *Nbeal2*^{-/-} MKs. We measured plasma concentration of granule proteins such as VWF and fibrinogen and found no difference between *Nbeal2*^{-/-} and control samples (data not shown) which was also reported in previous studies^{31,32} but this does not exclude a paracrine effect of the “leaking” granule proteins within the bone marrow potentially contributing to the pro-inflammatory effects of the MKs mentioned above and the development of myelofibrosis.

The observation of α -granules within the *Nbeal2*^{-/-} MKs is in contrast with the previously published mouse studies, which used a different knock-down strategy to our own. We can however draw a parallel to the few reported studies of MKs isolated from humans with GPS: some studies report the absence of α -granules in the MKs^{35,36} whilst others showed the presence of abnormal α -granules in the MKs by immunolabelling³⁷ further confirmed by EM³⁸. Indeed, Suppl Fig 9 illustrates MKs from a patient with GPS (carrying the mutation L388P in *NBEAL2*) that does contain granules just as it is the case for the mouse MKs reported here. One possible explanation for these differences would be sample preparation and in particular the level of maturity of the MKs analysed (culture-derived vs extracted from bone marrow, immature cells vs proplatelet forming MKs). We cannot rule out that these differences are explained by the variation in genotype between patients. Mutations in human *NBEAL2* have been found to affect different domains of the NBEAL2 protein, which may lead to a spectrum of phenotypes within the MKs whilst the end product, the platelets, is universally depleted of α -granules. A better understanding of the hitherto unknown function of the NBEAL2 protein and of its partners will be crucial in shedding light on how its deficiency/dysfunction affects α -granule formation and retention within the cell.

The clear demonstration that a lack of platelet α -granules has a link with a non-hemostatic platelet function led us to investigate whether the same was true for the role of platelets in

malignancies. To this end we used an *in vivo* model of cancer metastasis. Although this model addresses chiefly homing and invasion of malignant cells into tissue in the somewhat artificial context of large numbers of cells directly injected into the blood stream, the striking data place the platelet, and in particular its α -granules, at the center of the metastatic process. The rate of metastasis was markedly decreased in *Nbeal2*^{-/-} animals but remarkably, although transfusion with 240x10⁶ platelets only raised the platelet count by up to 15% of the *Nbeal2*^{-/-} baseline count, the rate of metastasis was almost restored to the levels observed in control mice. This observation makes it unlikely that the reduction in the platelet count of the *Nbeal2*^{-/-} mice is responsible for the decreased in metastasis observed but rather that it is their qualitative difference i.e. absence of α -granules that is the root cause for these results. The role of platelets in the spread of solid tumors is abundantly proven and different mechanisms have been put forward to explain this³⁹. Clinical implications of this phenomenon have been clearly demonstrated in a recent study showing a protective effect of low-dose “anti-platelet” aspirin for colon cancer⁷. P-selectin has been shown to be a key mediator in the formation of platelet-tumor cell aggregates promoting tumor metastasis⁴⁰⁻⁴³, and, P-selectin deficient mice are protected against cancer spread⁴⁴⁻⁴⁶. The lack of P-selectin expression on the surface of activated *Nbeal2*^{-/-} platelets provides a plausible explanation for the observation reported here, although we cannot exclude that other factors such as the lack of growth factors and pro-angiogenic proteins normally stored in the platelet α -granules could play a role. The majority of platelet transfusions to patients are carried out in the context of cancer treatment. The generation of platelets *in vitro* for clinical use is fast becoming a real prospect⁴⁷. It is not impossible to consider that informed by such models as described here, we could genetically modify stem cells so that their platelet progeny contain granules that preserve their haemostatic function whilst lowering their positive effect on metastasis⁴⁸.

In conclusion, we show that the pathogenicity of GPS extends beyond the absence of α -granules and a platelet hemostatic defect. We demonstrate an inflammatory component to the disease mediated, at least in part, by MKs, reflected by the development of myelofibrosis in older animals. We show evidence that Nbeal2 deficiency does not play a role in granule formation as such but in their retention within the MKs and platelets. Finally, we demonstrate in this mouse model for the first time a role for platelet α -granules in the metastatic spread of solid tumors.

Acknowledgements

We would like to acknowledge The Sanger Mouse genetics project. We thank JM Sowerby for sharing samples, and Jeremy Skepper and Simon McCallum for technical support on electron and confocal microscopy, respectively. This work was funded by the British Heart Foundation to CG (FS09/039) and WHO and AR (RG/09/12/28096); NHSBT to CB and HM; Wellcome Trust (WT098051) to ZM, ELC, JE, HWJ and AOS.

Authorship contribution

J.A.G., C.B., L.v.d.W., H.M. and M.C. performed experiments, analyzed data and edited the manuscript. P.N., A.O.S., W.N.E. and AR analyzed data and edited the manuscript. Z.M., E.L.C., J.E., H.W.J. and A.O.S generated the knockout mouse and prepared tissue samples. J.A.G., W.H.O and C.G. shared writing duties. J.A.G. and C.G. designed the study.

The authors declare no financial or other conflict of interest.

References

1. Semple JW, Italiano JE, Jr., Freedman J. Platelets and the immune continuum. *Nat Rev Immunol.* 2011;11(4):264-274.
2. Kisucka J, Butterfield CE, Duda DG, et al. Platelets and platelet adhesion support angiogenesis while preventing excessive hemorrhage. *Proc Natl Acad Sci U S A.* 2006;103(4):855-860.
3. Nurden AT, Nurden P, Sanchez M, Andia I, Anitua E. Platelets and wound healing. *Front Biosci.* 2008;13:3532-3548.
4. Jackson SP. Arterial thrombosis--insidious, unpredictable and deadly. *Nat Med.* 2011;17(11):1423-1436.
5. Boilard E, Nigrovic PA, Larabee K, et al. Platelets amplify inflammation in arthritis via collagen-dependent microparticle production. *Science.* 2010;327(5965):580-583.
6. Gay LJ, Felding-Habermann B. Contribution of platelets to tumour metastasis. *Nat Rev Cancer.* 2011;11(2):123-134.
7. Rothwell PM, Price JF, Fowkes FG, et al. Short-term effects of daily aspirin on cancer incidence, mortality, and non-vascular death: analysis of the time course of risks and benefits in 51 randomised controlled trials. *Lancet.* 2012;379(9826):1602-1612.
8. Coppinger JA, Cagney G, Toomey S, et al. Characterization of the proteins released from activated platelets leads to localization of novel platelet proteins in human atherosclerotic lesions. *Blood.* 2004;103(6):2096-2104.
9. Blair P, Flaumenhaft R. Platelet alpha-granules: basic biology and clinical correlates. *Blood Rev.* 2009;23(4):177-189.
10. Heijnen HF, Debili N, Vainchencker W, Breton-Gorius J, Geuze HJ, Sixma JJ. Multivesicular bodies are an intermediate stage in the formation of platelet alpha-granules. *Blood.* 1998;91(7):2313-2325.

11. Patel SR, Hartwig JH, Italiano JE, Jr. The biogenesis of platelets from megakaryocyte proplatelets. *J Clin Invest*. 2005;115(12):3348-3354.
12. Ambrosio AL, Boyle JA, Di Pietro SM. Mechanism of platelet dense granule biogenesis: study of cargo transport and function of Rab32 and Rab38 in a model system. *Blood*. 2012;120(19):4072-4081.
13. Raccuglia G. Gray platelet syndrome. A variety of qualitative platelet disorder. *Am J Med*. 1971;51(6):818-828.
14. Albers CA, Cvejic A, Favier R, et al. Exome sequencing identifies NBEAL2 as the causative gene for gray platelet syndrome. *Nat Genet*. 2011;43(8):735-737.
15. Kahr WH, Hinckley J, Li L, et al. Mutations in NBEAL2, encoding a BEACH protein, cause gray platelet syndrome. *Nat Genet*. 2011;43(8):738-740.
16. Gunay-Aygun M, Falik-Zaccai TC, Vilboux T, et al. NBEAL2 is mutated in gray platelet syndrome and is required for biogenesis of platelet alpha-granules. *Nat Genet*. 2011;43(8):732-734.
17. Maynard DM, Heijnen HF, Gahl WA, Gunay-Aygun M. The alpha-granule proteome: novel proteins in normal and ghost granules in gray platelet syndrome. *J Thromb Haemost*. 2010;8(8):1786-1796.
18. Nurden AT, Nurden P. The gray platelet syndrome: clinical spectrum of the disease. *Blood Rev*. 2007;21(1):21-36.
19. Nagle DL, Karim MA, Woolf EA, et al. Identification and mutation analysis of the complete gene for Chediak-Higashi syndrome. *Nat Genet*. 1996;14(3):307-311.
20. Castermans D, Volders K, Crepel A, et al. SCAMP5, NBEA and AMISYN: three candidate genes for autism involved in secretion of large dense-core vesicles. *Hum Mol Genet*. 2010;19(7):1368-1378.

21. Skarnes WC, Rosen B, West AP, et al. A conditional knockout resource for the genome-wide study of mouse gene function. *Nature*. 2011;474(7351):337-342.
22. White JK, Gerdin AK, Karp NA, et al. Genome-wide generation and systematic phenotyping of knockout mice reveals new roles for many genes. *Cell*. 2013;154(2):452-464.
23. Ryder E, Gleeson D, Sethi D, et al. Molecular characterization of mutant mouse strains generated from the EUCOMM/KOMP-CSD ES cell resource. *Mamm Genome*. 2013;24(7-8):286-294.
24. Hobbs CM, Manning H, Bennett C, et al. JAK2V617F leads to intrinsic changes in platelet formation and reactivity in a knock-in mouse model of essential thrombocythemia. *Blood*. 2013.
25. Guerrero JA, Kyei M, Russell S, et al. Visualizing the von Willebrand factor/glycoprotein Ib-IX axis with a platelet-type von Willebrand disease mutation. *Blood*. 2009;114(27):5541-5546.
26. Subramanian A, Tamayo P, Mootha VK, et al. Gene set enrichment analysis: a knowledge-based approach for interpreting genome-wide expression profiles. *Proc Natl Acad Sci U S A*. 2005;102(43):15545-15550.
27. Sehgal S, Storrie B. Evidence that differential packaging of the major platelet granule proteins von Willebrand factor and fibrinogen can support their differential release. *J Thromb Haemost*. 2007;5(10):2009-2016.
28. Tefferi A, Vaidya R, Caramazza D, Finke C, Lasho T, Pardanani A. Circulating interleukin (IL)-8, IL-2R, IL-12, and IL-15 levels are independently prognostic in primary myelofibrosis: a comprehensive cytokine profiling study. *J Clin Oncol*. 2011;29(10):1356-1363.
29. Hasselbalch HC. The role of cytokines in the initiation and progression of myelofibrosis. *Cytokine Growth Factor Rev*. 2013;24(2):133-145.

30. Acharyya S, Oskarsson T, Vanharanta S, et al. A CXCL1 paracrine network links cancer chemoresistance and metastasis. *Cell*. 2012;150(1):165-178.
31. Deppermann C, Cherpokova D, Nurden P, et al. Gray platelet syndrome and defective thrombo-inflammation in Nbeal2-deficient mice. *J Clin Invest*. 2013.
32. Kahr WH, Lo RW, Li L, et al. Abnormal megakaryocyte development and platelet function in Nbeal2^{-/-} mice. *Blood*. 2013;122(19):3349-3358.
33. Pardanani A, Vannucchi AM, Passamonti F, Cervantes F, Barbui T, Tefferi A. JAK inhibitor therapy for myelofibrosis: critical assessment of value and limitations. *Leukemia*. 2011;25(2):218-225.
34. Schmitt A, Jouault H, Guichard J, Wendling F, Drouin A, Cramer EM. Pathologic interaction between megakaryocytes and polymorphonuclear leukocytes in myelofibrosis. *Blood*. 2000;96(4):1342-1347.
35. White JG. Ultrastructural studies of the gray platelet syndrome. *Am J Pathol*. 1979;95(2):445-462.
36. Breton-Gorius J, Vainchenker W, Nurden A, Levy-Toledano S, Caen J. Defective alpha-granule production in megakaryocytes from gray platelet syndrome: ultrastructural studies of bone marrow cells and megakaryocytes growing in culture from blood precursors. *Am J Pathol*. 1981;102(1):10-19.
37. Falik-Zaccai TC, Anikster Y, Rivera CE, et al. A new genetic isolate of gray platelet syndrome (GPS): clinical, cellular, and hematologic characteristics. *Mol Genet Metab*. 2001;74(3):303-313.
38. Cramer EM, Vainchenker W, Vinci G, Guichard J, Breton-Gorius J. Gray platelet syndrome: immunoelectron microscopic localization of fibrinogen and von Willebrand factor in platelets and megakaryocytes. *Blood*. 1985;66(6):1309-1316.

39. Jain S, Harris J, Ware J. Platelets: linking hemostasis and cancer. *Arterioscler Thromb Vasc Biol.* 2010;30(12):2362-2367.
40. Cooney CA, Jousheghany F, Yao-Borengasser A, et al. Chondroitin sulfates play a major role in breast cancer metastasis: a role for CSPG4 and CHST11 gene expression in forming surface P-selectin ligands in aggressive breast cancer cells. *Breast Cancer Res.* 2011;13(3):R58.
41. Garcia J, Callewaert N, Borsig L. P-selectin mediates metastatic progression through binding to sulfatides on tumor cells. *Glycobiology.* 2007;17(2):185-196.
42. Monzavi-Karbassi B, Stanley JS, Hennings L, et al. Chondroitin sulfate glycosaminoglycans as major P-selectin ligands on metastatic breast cancer cell lines. *Int J Cancer.* 2007;120(6):1179-1191.
43. Borsig L, Wong R, Feramisco J, Nadeau DR, Varki NM, Varki A. Heparin and cancer revisited: mechanistic connections involving platelets, P-selectin, carcinoma mucins, and tumor metastasis. *Proc Natl Acad Sci U S A.* 2001;98(6):3352-3357.
44. Kohler S, Ullrich S, Richter U, Schumacher U. E-/P-selectins and colon carcinoma metastasis: first in vivo evidence for their crucial role in a clinically relevant model of spontaneous metastasis formation in the lung. *Br J Cancer.* 2010;102(3):602-609.
45. Borsig L, Wong R, Hynes RO, Varki NM, Varki A. Synergistic effects of L- and P-selectin in facilitating tumor metastasis can involve non-mucin ligands and implicate leukocytes as enhancers of metastasis. *Proc Natl Acad Sci U S A.* 2002;99(4):2193-2198.
46. Kim YJ, Borsig L, Varki NM, Varki A. P-selectin deficiency attenuates tumor growth and metastasis. *Proc Natl Acad Sci U S A.* 1998;95(16):9325-9330.
47. Avanzi MP, Mitchell WB. Ex vivo production of platelets from stem cells. *Br J Haematol.* 2014;165(2):237-247.

48. Italiano JE, Jr., Battinelli EM. Selective sorting of alpha-granule proteins. *J Thromb Haemost.* 2009;7 Suppl 1:173-176.

Figure Legends

Figure 1. Deficiency of *Nbeal2* in mice leads to Gray Platelet Syndrome. (A) Transcript levels of *Nbeal2* by qPCR in RNA isolated from *in vitro*-cultured megakaryocytes. Results are normalised to levels of GP6 (n=3). (B) Protein levels of Nbeal2 in platelets and megakaryocytes from *Nbeal2*^{-/-} and control mice. β -actin included as an internal loading control (n=3). (C) Platelet count in *Nbeal2*^{-/-} and control animals (n=13). (D) Mean platelet volume in *Nbeal2*^{-/-} and control mice (n=13). (E) Size distribution of the gated platelet population visualised in a representative flow cytometry histogram (Forward-scatter). (F) Representative May-Grünwald Giemsa stain of blood smears. Arrows indicate the presence of platelets. Platelets are larger and appear grey in *Nbeal2*^{-/-} samples. Scale bar: 20 μ m. (G) Different degrees of splenomegaly were observed in *Nbeal2*^{-/-} mice beyond the age of 9 months. Age-matched control mice were used for comparison (n=4). (H) A representative reticulin staining of bone sections from mice at 9 months of age showing myelofibrosis in *Nbeal2*^{-/-} marrow. Scale bar: 200 μ m.

Figure 2. Impaired platelet function in *Nbeal2*^{-/-} mice. (A,B) Ultrastructure of platelets from control mice showing abundant α -granules (AG), among other organelles. (C,D) Ultrastructure of *Nbeal2*^{-/-} platelets showing a significant reduction of α -granules, several vacuoles (V) and membrane inclusions (MI). (E-F) Immunolabelling of VWF (red) and CD41 (green) in control (E) and *Nbeal2*^{-/-} (F) platelets. Images correspond to the maximum intensity projections of an image stack across an entire platelet section. A higher magnification of the circled platelets is shown for clarification. VWF is restricted to the α -granules in control platelets while its distribution is more diffuse in *Nbeal2*^{-/-} platelets. Note

also the absence of VWF in some *Nbeal2*^{-/-} platelets. (G) Representative immunoblots of α -granule proteins von Willebrand Factor (VWF), thrombospondin-1 (THBS1) and platelet factor 4 (PF4) in control and *Nbeal2*^{-/-} platelet lysates. CD63 (LAMP-3), a lysosomal/dense granule marker, and β -actin and GAPDH included as loading controls. Bottom graphs show the densitometry analysis performed using ImageJ (n=3). (H) Flow cytometry analysis of platelet activation induced by 1 μ g/mL collagen-related peptide (CRP) and 1 U/mL thrombin (n=4) showing equivalent fibrinogen binding to *Nbeal2*^{-/-} and control platelets (top panel, only shown for CRP), in contrast reduced P-selectin exposure in *Nbeal2*^{-/-} platelets with both agonists (middle and bottom panels). Plots with vertical lines correspond to basal platelet activation in the absence of agonist. For all graphs, bars represent mean \pm SEM. N.S.: non-significant. MFI: Mean Fluorescent Intensity. Scale Bar: 100 nm (A, C) and 500 nm (B, D). * P-value<0.05.

Figure 3. Abnormal MK maturation in *Nbeal2*^{-/-} mice. (A) CD41 labelling and H&E staining of bone sections (60x) in control and *Nbeal2*^{-/-} mice. Arrows point at MKs. Two representative large polyploid MKs are shown in the bottom panels at high magnification (100x). Note the presence of leukocytes (L) within MKs (emperipolesis) at high magnification (100x) in the *Nbeal2*^{-/-} samples. (B) Quantitation of MKs in bone sections from A (5 different fields in 5 mice). Similar total MK numbers in control and *Nbeal2*^{-/-} mice (top panel) but the numbers of large MKs with more than 2 nuclear lobes (middle panel) and numbers of small MKs with 2 or less nuclear lobes (bottom panel) are significantly different in *Nbeal2*^{-/-} mice. (C) Percentage of CD41⁺ cells in bone marrow cultures in the presence of thrombopoietin (TPO) (1 and 5 ng/mL) at different time points (1, 3 and 5 days) (n=4). (D) Ploidy profile of CD41⁺ cells at day 3 (n=4). (E) Percentage of proplatelet forming

megakaryocytes upon adhesion to fibrinogen of cultured megakaryocytes purified by BSA gradient (n=4). For all graphs, bars represent mean±SEM. * p<0.05.

Figure 4. Ultrastructure and protein analysis of megakaryocytes. (A-D) Ultrastructure of culture-derived megakaryocytes from control (A) and *Nbeal2*^{-/-} (B) mice at low magnification (A, B) and high magnification (C, D), respectively. Multivesicular bodies (MVB), precursors of α -granules, are present in both control and *Nbeal2*^{-/-} megakaryocytes. (E, F) Ultrastructure of bone marrow megakaryocytes in control and *Nbeal2*^{-/-} animals at low magnification. (G, H, I, J) Ultrastructure of bone marrow megakaryocytes from control and *Nbeal2*^{-/-} mice at high magnification. A well-defined demarcation membrane system with the presence of platelet territories and α -granules (AG) in control cells (G, I). The demarcation membrane system in *Nbeal2*^{-/-} megakaryocytes is not well-defined (H, J), however, α -granules (AG) are present. (K) Low magnification of a proplatelet-forming MK from *Nbeal2*^{-/-} bone marrow. (L) A high magnification of the circled area in K highlights the presence of α -granules (AG) inside the emerging platelet fields, and vacuoles (V) within the MK cytoplasm. (M) Representative immunoblots of α -granule proteins (VWF, thrombospondin-1 and PF4) in control and *Nbeal2*^{-/-} MKs. CD63 (LAMP-3), a lysosomal/dense granule marker, and β -actin and GAPDH included as loading controls. Below, graphs show the densitometry analysis performed using ImageJ (n=3). Bars represent mean±SEM. N.S.: non-significant. Scale bar: 2 μ m (A, B, E, F, K), 500 nm (C, D, G, H, I, J, L). Representative images were selected from 5 different mice per group.

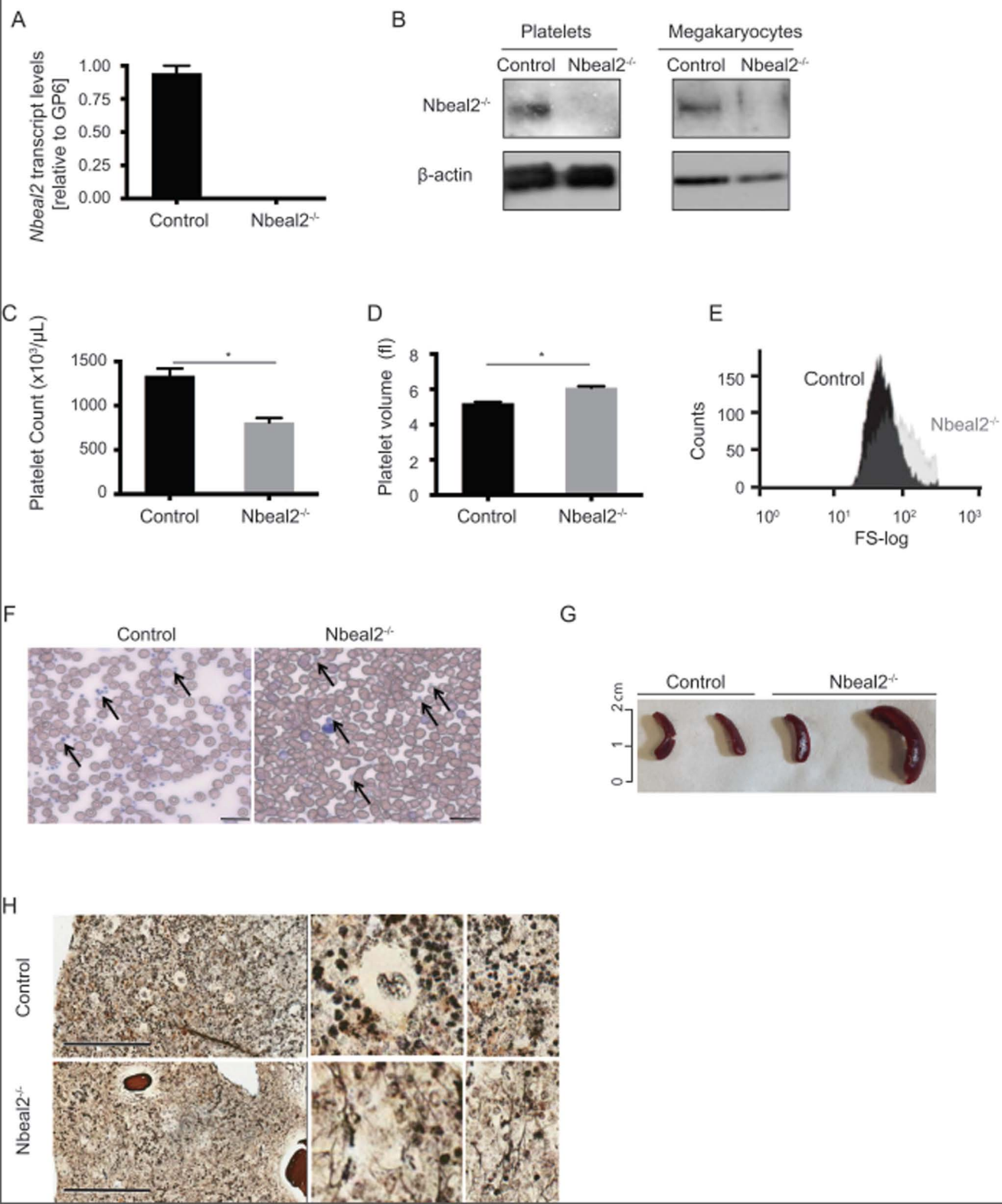
Figure 5. Analysis of α -granules and their content in proplatelet-forming megakaryocytes by electron and confocal microscopy. (A) Low magnification of a representative control proplatelet-forming megakaryocyte by SEM showing proplatelet-like

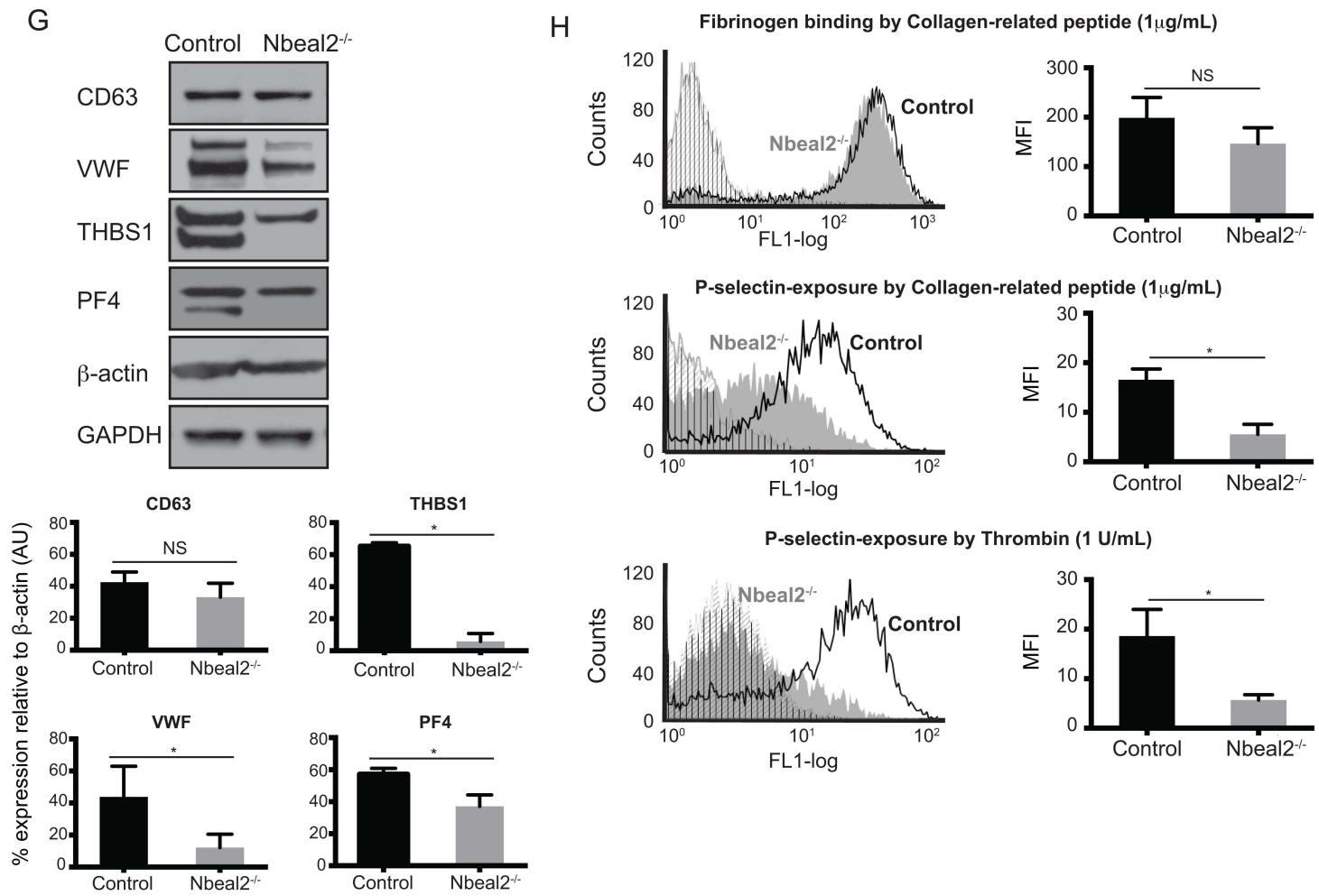
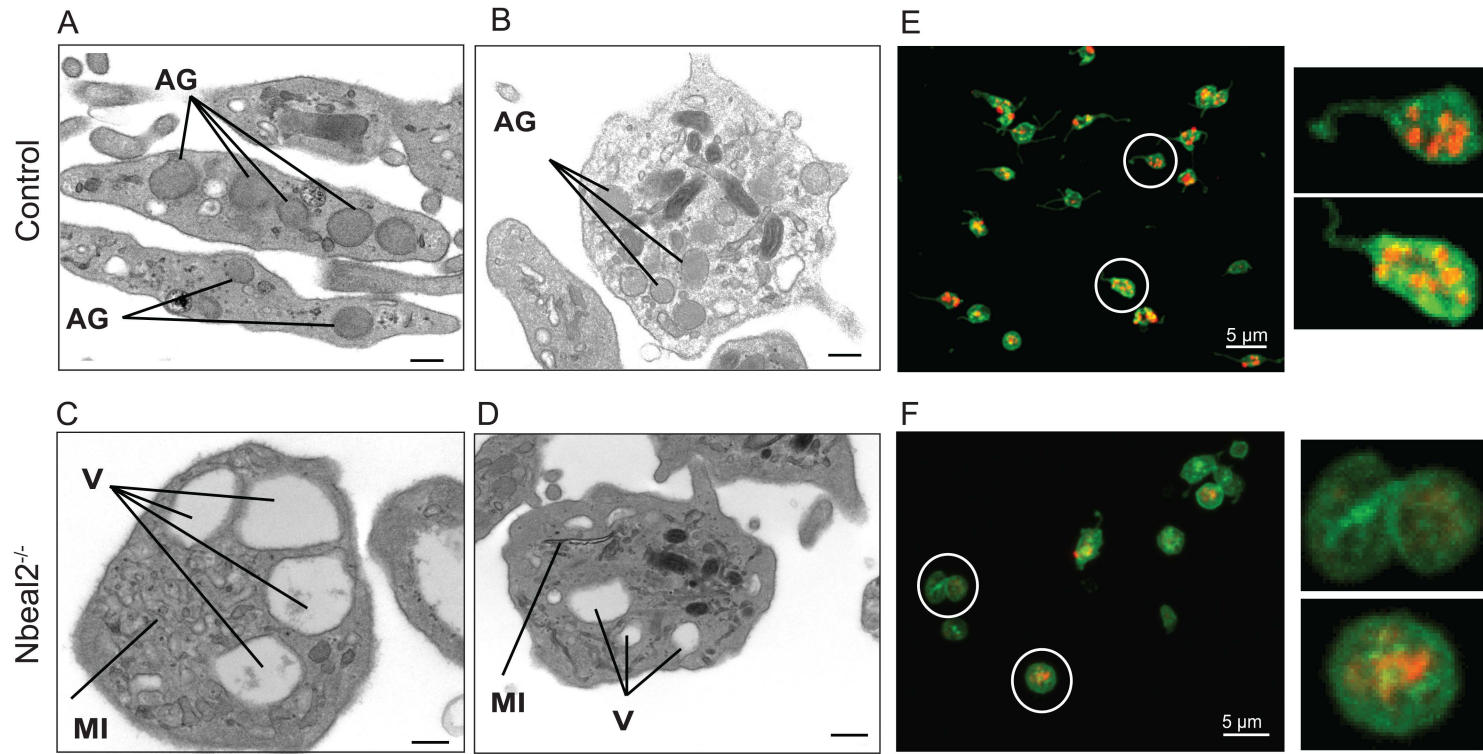
territories emerging from the main core of the cell. (B, C). Higher magnification of the circled areas in A seen by TEM. The developing proplatelets contain multivesicular bodies (MVB), precursors of α -granules. (D, E) Immunolabelling of CD41 and VWF in proplatelet-forming megakaryocytes by confocal microscopy in control (D) and *Nbeal2*^{-/-} (E) cells. VWF is restricted to the multivesicular bodies observed in B and C. The inset at the top-right corner in E highlights the presence of a thin MK filament bridging several emerging platelet-like particles. (F, G) Immunolabelling of CD41 in proplatelet-forming megakaryocytes previously cultured in the presence of FITC-Fibrinogen. Fibrinogen is endocytosed and packaged into α -granules in control (F) and *Nbeal2*^{-/-} (G) megakaryocytes, and transported through the proplatelet shafts. (H, I) Proplatelet-forming megakaryocytes cultured with FITC-Fibrinogen as stated in F, and P-selectin-immunolabelled in control (H) and *Nbeal2*^{-/-} (I) samples. (J, K) Proplatelet-forming megakaryocytes cultured in the presence of FITC-fibrinogen as stated in F, and VWF-immunolabelled in control (J) and *Nbeal2*^{-/-} (K) samples. (L) Quantitation of proplatelets bud in MK culture. (M) Percentage of proplatelets buds containing the α -granule protein VWF. For each panel, the insets represent a higher magnification of platelet-like particles showing a similar granular distribution of P-selectin, VWF and fibronogen in control and *Nbeal2*^{-/-} cells. For panels D-K, the nucleus was stained with DAPI (blue). Representative images were selected from 5 different mice per group.

Figure 6. Gene expression array in culture-derived megakaryocytes. (A) Enrichment of the “Chemokine activity” gene set in *Nbeal2*^{-/-} megakaryocytes with the genes contributing to this enrichment. (B) Fold change of the 6 most significant genes identified in A in *Nbeal2*^{-/-} versus control MKs generated by q-PCR using different samples as those used in the array (n=3). (C) Plasma levels of the chemokines MIP-1 α (*Ccl3*), MIP-1 β (*Ccl4*) and Cxcl1 in MK

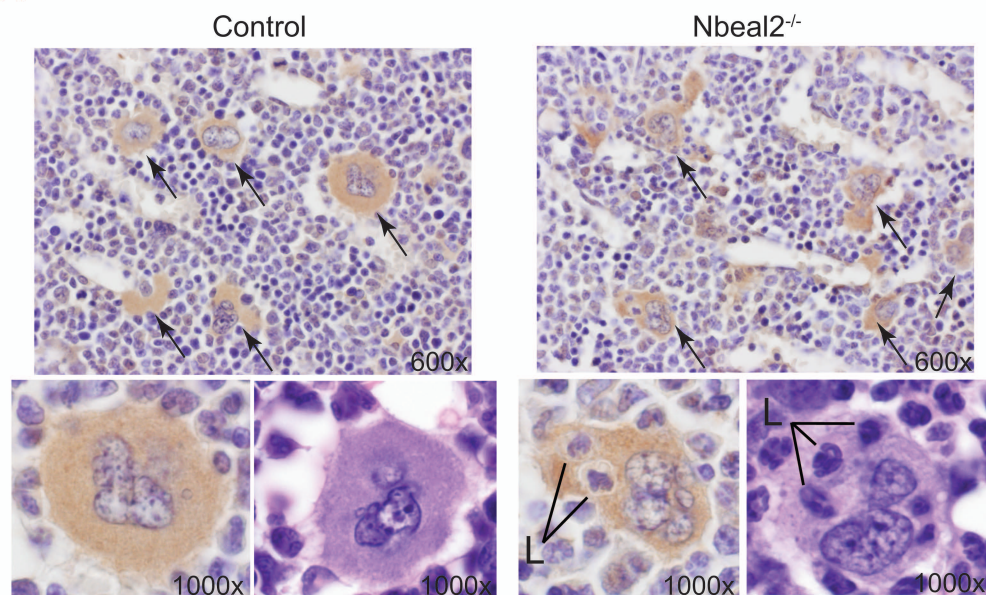
culture supernatant. (D) Levels of these chemokines in plasma of control and *Nbeal2*^{-/-} mice (n=5). Bars represent mean±SEM. * p<0.05.

Figure 7. Reduced metastasis in *Nbeal2*^{-/-} mice. Lung metastasis was induced by tail vein injection of 5 x 10⁵ mouse melanoma B16-F10 cells. Lungs were taken after 10 days and the number of pulmonary metastases counted on all 5 lobes of the lung. Representative lung metastases in control (n=9) and *Nbeal2*^{-/-} mice (n=5) (left panel) and quantitation (right panel). Bars represent mean±SEM. * p=0.0001.

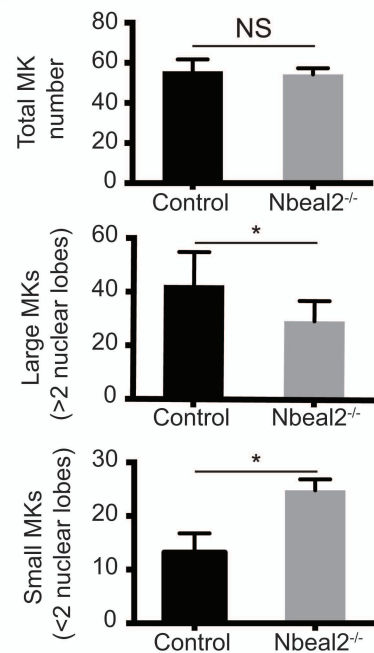




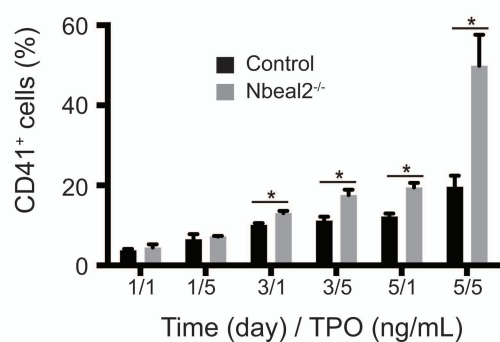
A



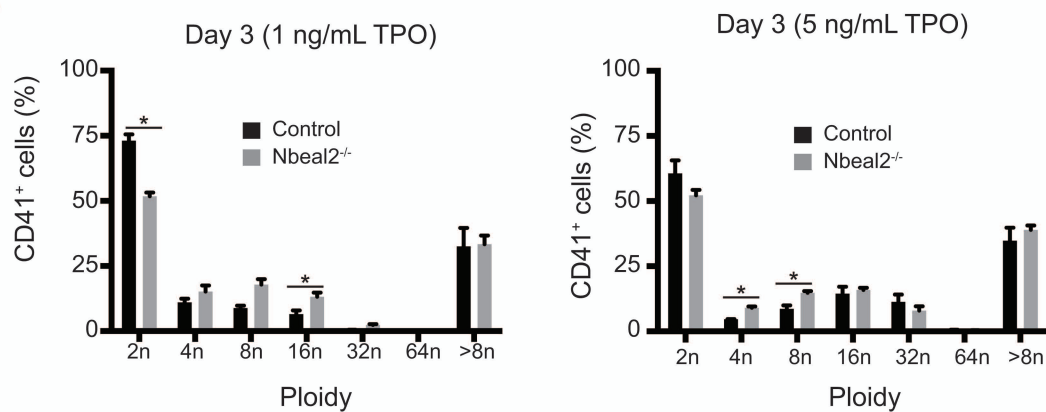
B



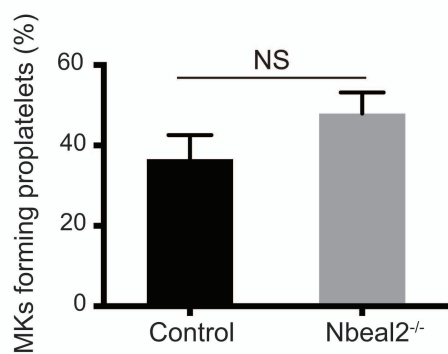
C

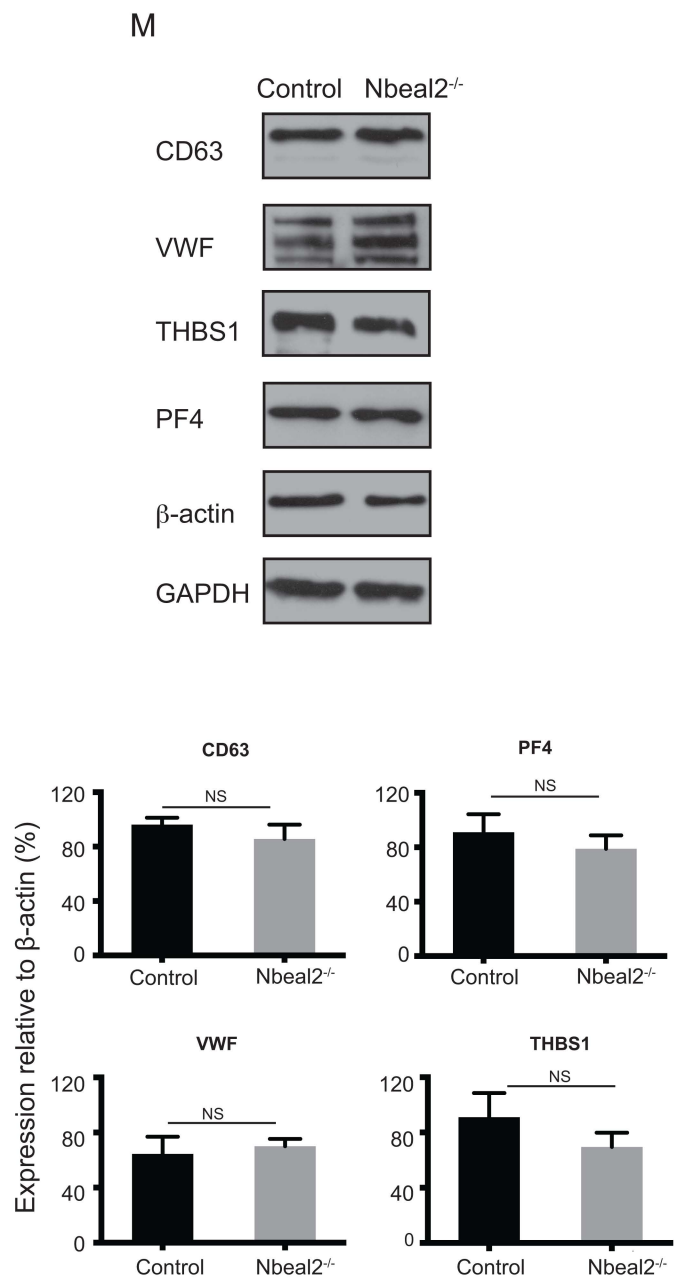
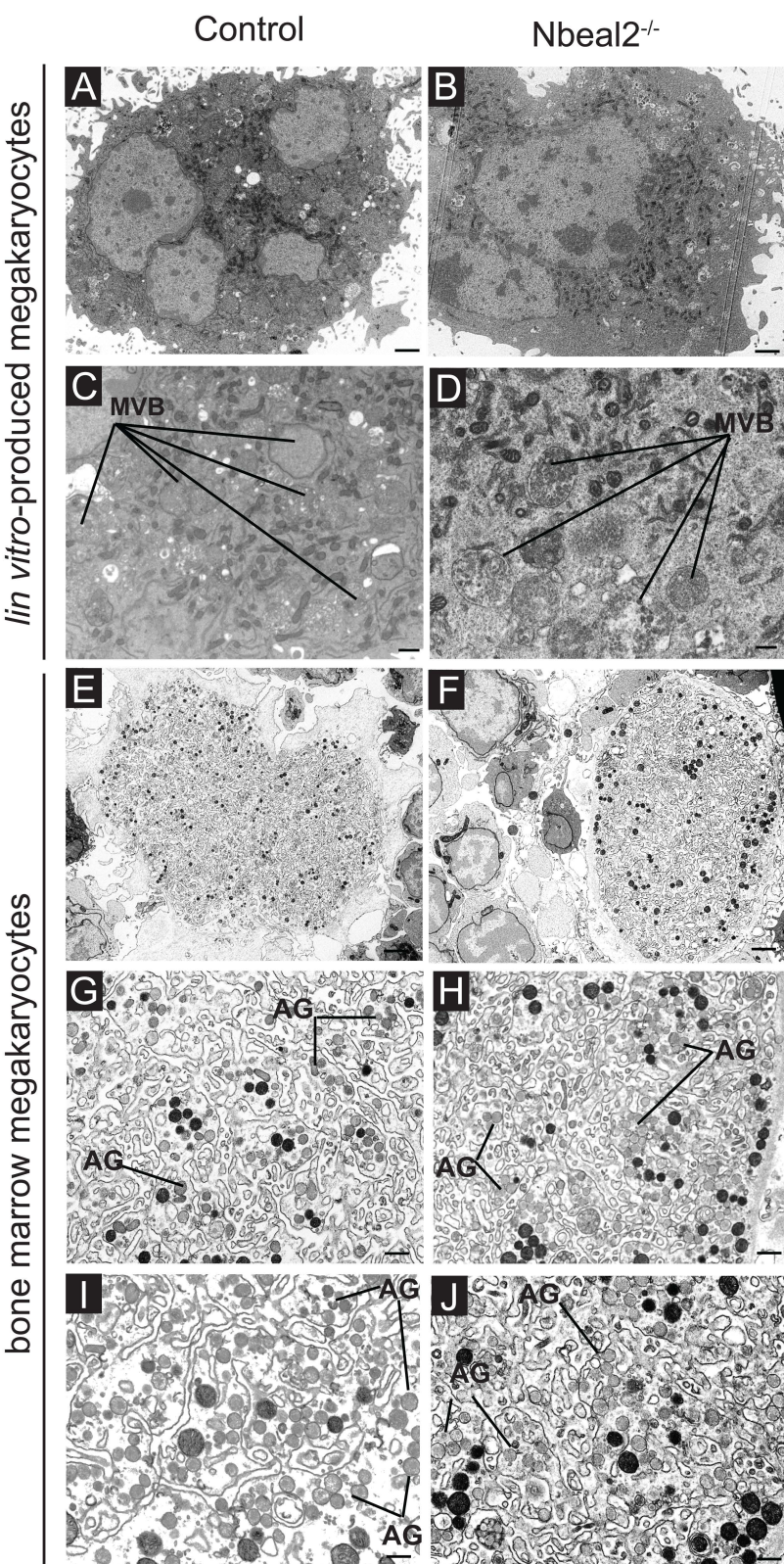
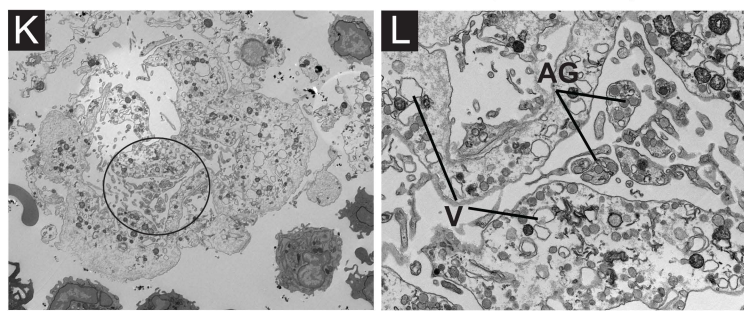


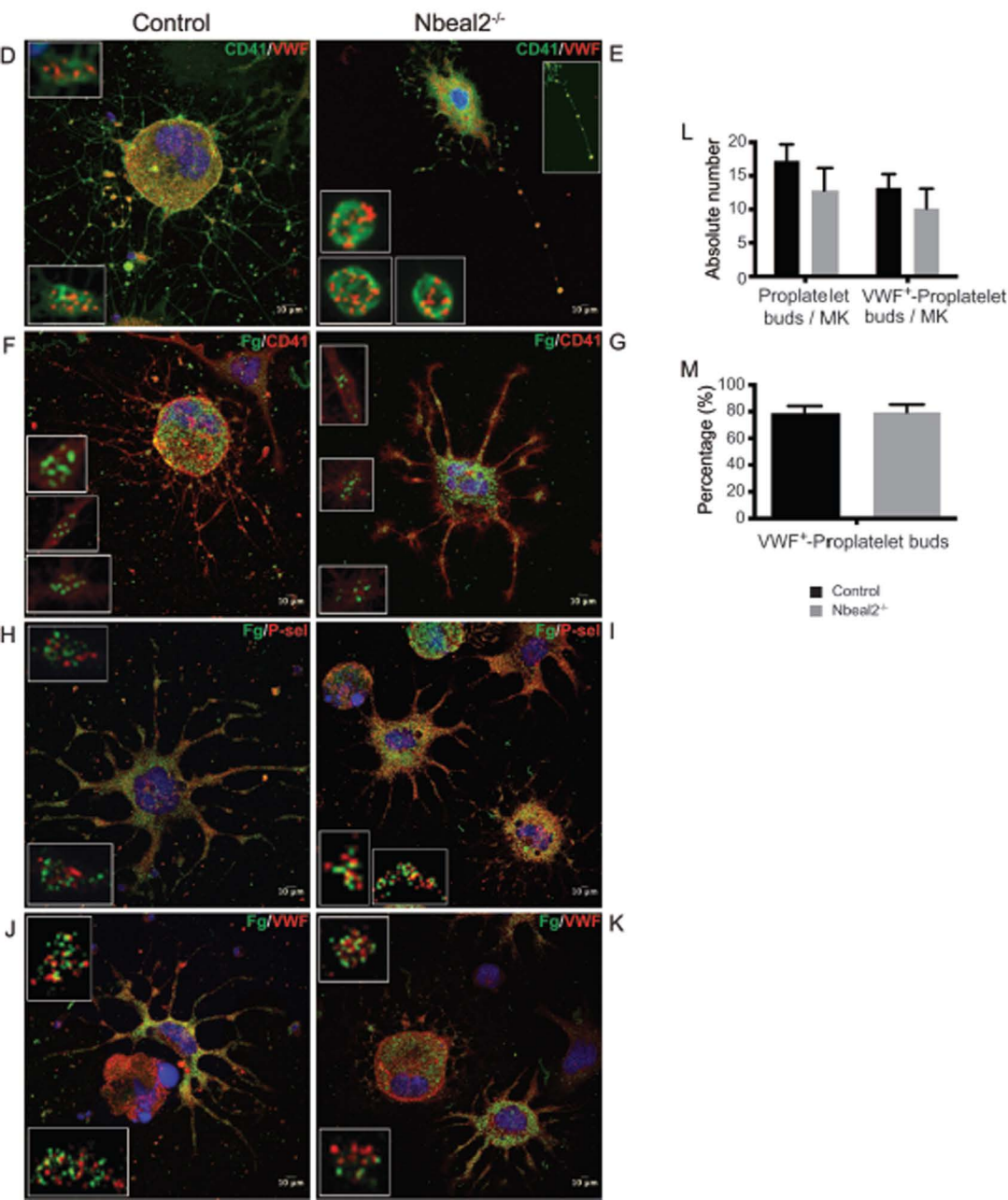
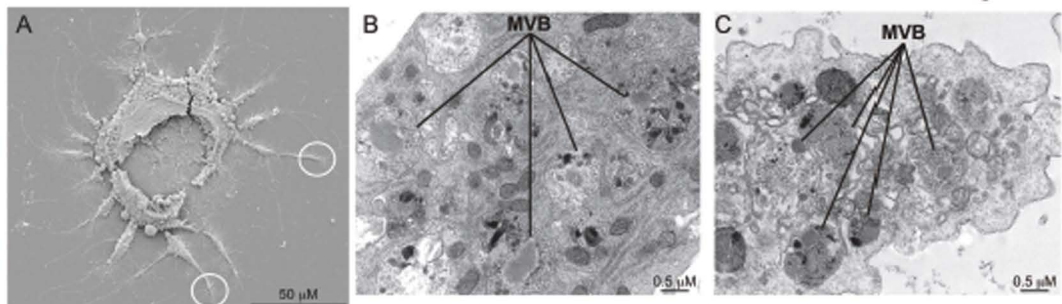
D



E



bone marrow proplatelet (Nbeal2^{-/-})



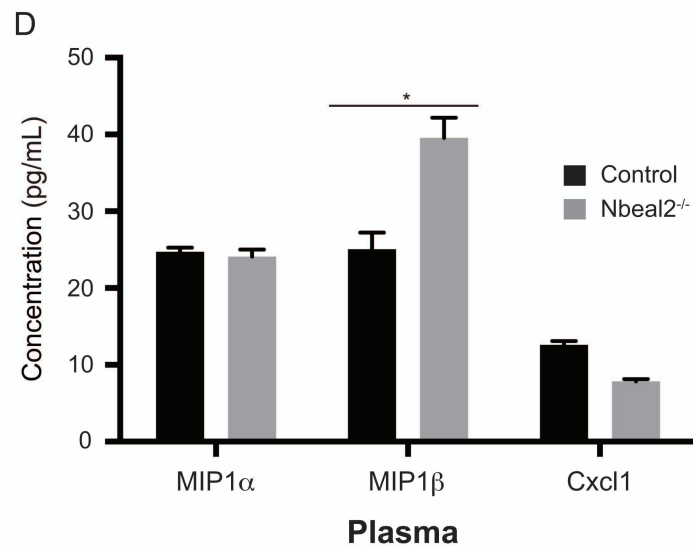
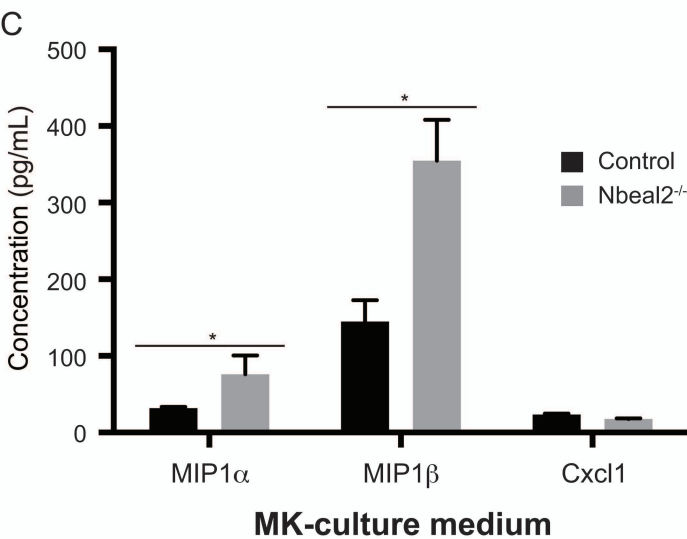
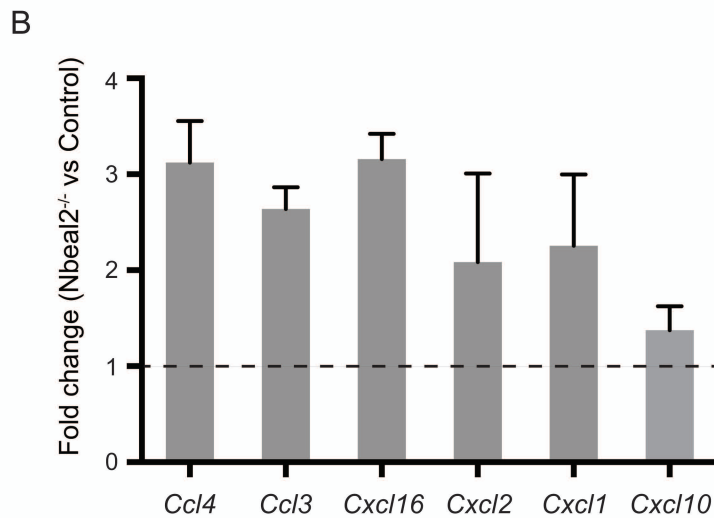
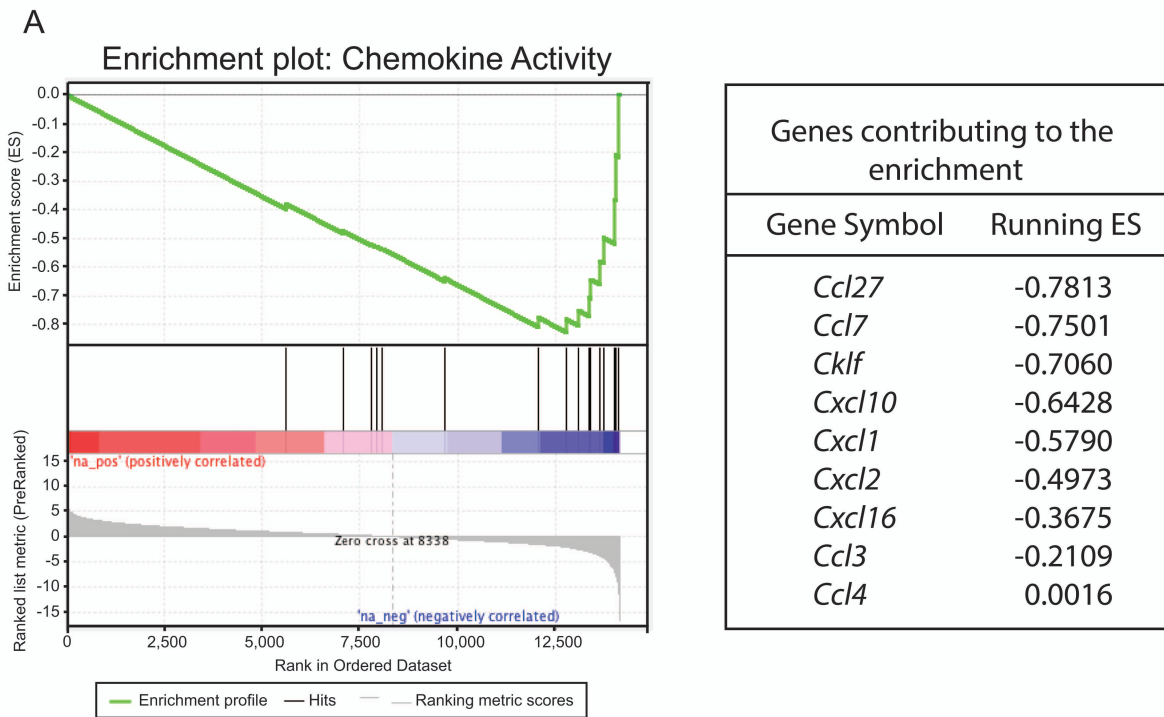


Figure 7

Control

Nbeal2^{-/-}

